

## Determining diazinon degradation using potassium hydrogen monopersulfate and magnetic copper ferrite nano-particles in contact with ozone in aqueous solutions

Seyed Jamshid Moosavi<sup>a</sup>, Abdolrahim Pazira<sup>a,\*</sup>, Taebeh Tabatabaie<sup>a</sup>,  
Neematollah Jaafarzadeh<sup>a,b</sup>, Sahand Jorfi<sup>a,c</sup>

<sup>a</sup>Department of Environment, Bushehr Branch, Islamic Azad University, Bushehr, Iran, Tel. +989173723932; email: pazira@iaubusheher.ac.ir (A. Pazira), Tel. +989176388066; email: sj.moosavi@gmail.com (S.J. Moosavi), Tel. +989177733623; email: tabatabaiett20@gmail.com (T. Tabatabaie), Tel. +989163184501; email: Jaafarzadeh-n@ajums.ac.ir (N. Jaafarzadeh), Tel. +989163109153; email: sahand369@yahoo.com (S. Jorfi)

<sup>b</sup>Toxicology Research Center, Ahvaz Jundishapur University of Medical Sciences, Ahvaz, Iran

<sup>c</sup>Department of Environmental Health Engineering, Ahvaz Jundishapur University of Medical Sciences, Ahvaz, Iran

Received 16 December 2019; Accepted 28 November 2020

### ABSTRACT

In this paper, magnetic copper ferrite nano-particles ( $\text{CuFe}_2\text{O}_4$ , MNPs) are applied in the ozone/potassium hydrogen monopersulfate (KMPS) system to degrade diazinon pesticide (DZN). To do so, the features of MNPs, the factors affecting the system, and the kinetic of the reaction are investigated. In this matter, the KMPS/MNPs/ozone system is able to degrade 20 mg/L of DZN completely in 20 min under the conditions of 6 mg/L ozone, 0.6 g/L KMPS, 0.1 g/L MNPs in pH = 7. The obtained results pertaining to reusability and stability verify that MNPs can be utilized in this system under several times without losing its catalytic activity. Moreover, both KMPS and ozone increase copper and iron chelation. Various single, binary, and ternary systems of ozone/KMPS/MNPs are assessed in the DZN degradation. The effectiveness of the process is assessed in the existence of different types of anions toward the conclusion, in which bicarbonate has the highest whereas nitrate has the lowest scavenging. Additionally, some decreases in the degradation can be observed while the process in several different real situations is surveyed. Furthermore, the effective agents in the scavenging experiments prove to play a role in degradation of DZN such as sulfate radical and hydroxyl radical. Mineralization of diazinon in the process is evaluated via the total organic carbon (TOC) parameter in the ozone/MNPs/KMPS system. As expected, the mineralization occurs with the elimination of 61%/9% of TOC. Ultimately, the by-products of the process are analyzed using gas chromatography–mass spectrometry.

**Keywords:** Copper ferrite; Ozone; Potassium hydrogen monopersulfate; Pesticide

### 1. Introduction

Agricultural pests are reckoned amongst the most important issues preventing the growth of trees and plants.

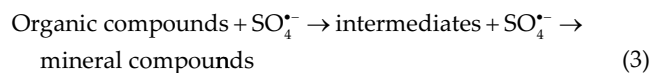
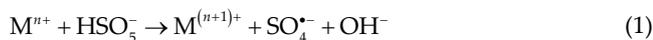
The most frequent way to eliminate them may be the use of chemical pesticides as DZN. DZN is a contact phosphorus compound applied both in the soil and on the aerial organs of plants. Having been used in fighting against rice stemborers in the north of Iran since 1977, this insecticide

\* Corresponding author.

has been of the highest consumption among the pesticides (more than 10% of all) used in Iran in 2010 [1]. DZN has wide application and is used against domestic insects, garden pests, ornamental plants, pets, and even flies and mosquitoes in stables [2]. It is also applied in spraying garden parks [3]. Chemicals like DZN may be conducive to increasing food products; however, their waste may be found in groundwater and rivers causing many problems for the ecosystem and human beings. Accordingly, researchers explore ways to prevent and check such agricultural chemicals, which are resistant to biotic decomposition for a long time, and at very low concentrations, they may have irretrievable effects on human health [4–8].

Despite being inexpensive and ecofriendly among others, biological treatment may not be able to totally degrade the pesticides owing to their toxicity for microorganisms [9]. Degradation of persistent organic contaminants via free radicals may be the outcome of advanced oxidation processes (AOPs). In this regard, to degrade organic compounds many techniques, such as catalytic ozonation, photocatalysis, electrochemical processes, and Fenton oxidation are applied in order to create hydroxyl radicals with the redox potential of 2.8 V [10]. Various combinations of AOPs are known as gifted ways to degrade contaminants [11]. Earlier, sulfate radical-based AOPs have been used in preference to hydroxyl radical-based AOPs like longer half time and higher redox potential ( $E_0 = 2.5\text{--}3.1$  V) of sulfate radical [12,13]. Various methods may be applied to activate the chemical oxidants of potassium hydrogen monopersulfate (KMPS) and persulfate as precursors aiming at producing sulfate radicals. Thanks to its asymmetrical structure, KMPS ( $\text{HSO}_5^-$ ) is more straightforward than persulfate to be activated [14].

Various methods are applied to activate KMPS in order to produce sulfate radical from among them are heat, transition metals (iron, cobalt, and copper), ultraviolet rays [15,16], and ultrasonic waves [17]. Owing to its high frequency in the earth's crust and lower toxicity, iron has attracted researchers' attention more than the other transition metals [18,19].



Several studies have been conducted on degradation of pollutants by sulfate radical. Among others, the activation methods via transition metals in homogenic or heterogenic form have been used. The homogeneity having better performance is hard to recover. Furthermore, the heterogeneous process possesses the catalyst recover and avoids the transition metal [20]. A combination of two or more AOPs in a reactor is called an advanced oxidation hybrid process including cases such as photo-Fenton, sonophotocatalysis,  $\text{O}_3/\text{H}_2\text{O}_2/\text{UV}$ , photolysis, sonolysis, ozonation, and electro-Fenton. Hybrid processes are used to

increase efficiency, and nowadays various compounds of AOPs regarding the treatment of POPs and toxic materials have been studied [21,22]. Both oxidants ozone and KMPS could be activated as heterogene to produce hydroxyl radical and sulfate radical, respectively. The heterogenic catalysts are widely used in this respect and are categorized in the following three groups: (1) based on metals and metal oxides; (2) based on carbon; (3) composites of carbon and metals on different supports [23–25]. Among other heterogenic catalysts, metal oxides are positioned in higher conditions and are more noteworthy owing to reuse in several cycles. Although cobalt oxides have had the best function in KMPS activation, iron-based metal oxides are more applicable in this regard. Since certain iron oxides have magnetic properties, their separation from the solution is far easier. For instance,  $\text{Fe}_3\text{O}_4$ ,  $\gamma\text{-Fe}_2\text{O}_3$ , and  $(\text{FeO}(\text{OH}))$  are widely employed to activate hydrogen peroxide [26,27].

Recently, the usage of various spinels with the general formula  $(\text{AB}_2\text{O}_4)$  has been common to activate oxidants. Here, A and B are transition metals or alkaline earth metals [28,29]. The element B is usually regarded as iron known generally as ferrite. Ferrite nanoparticles are used mostly as absorbent, catalyst, and photocatalyst to curb environmental pollution. Magnetic copper ferrite nanoparticles  $\text{CuFe}_2\text{O}_4$  (magnetic nanoparticles (MNPs)) is another spinel extensively used for a long time in pharmaceutical and metallurgical industries, and has been mostly considered for AOPs owing to its high magnetic properties in the degradation of organic materials. Indeed, MNPs consist of hematite ( $\text{Fe}_2\text{O}_3$ ) and copper oxide (CuO) and have the property of both metal oxides. The redox cycle is facilitated by the presence of the oxidant, so that  $\text{Fe}^{2+}/\text{Fe}^{3+}$  and  $\text{Cu}^{2+}/\text{Cu}^{3+}$  can be converted to each other during the reaction [30,31].

As a catalyst, copper nanoferrite has been used for KMPS [30], persulfate [32], hydrogen peroxide [28], and ozone [33]. Through the active sites of Cu(II) in CuO and Fe(III) in  $\text{Fe}_2\text{O}_3$ , copper ferrite nanoparticles considerably contribute to the activation of oxidants. In recent years, the activation of oxidants by  $\text{CuFe}_2\text{O}_4$  MNPs has been the focus of researches [32,34]. Utilization of MNPs in coincident activation of KMPS and ozone has not been yet studied. Indeed, the use of one activator to catalyze two different oxidants has not been the subject of the investigation thus far in the sanitization of polluted waters. In this fashion, the interaction of the oxidants could have had a synergic impact on the catalyst nonattendance. Therefore, merging of ozone, MNPs and KMPS would be the incorporation of liquid–solid reaction (KMPS/MNPs), liquid–gas reaction (KMPS/ozone), and gas–solid reaction (ozone/MNPs) opening a new window in studies on the combination of AOPs.

In this research, a new-fangled tripartite blend of AOPs (KMPS/MNPs/ozone) was studied to degrade an insecticide (DZN). Effective factors of the process were investigated on the DZN degradation. Reusability and stability of MNPs were evaluated by recycling the catalyst and the leaching test. The systems achievement was assessed in different matrices (tap water and secondary effluent). To decide on mechanism, experiments of scavenging were conducted via several chemical explorations. Lastly, transformation of diazonin was recognized using the produced intermediates all through the degradation.

## 2. Materials and methods

### 2.1. Chemical substances

DZN ( $C_{12}H_{21}N_{20}O_3$ PS) (CAS number 333-41-5) was obtained from Sigma-Aldrich Co., (USA) KMPS, ethanol, and *tert*-butyl alcohol were acquired from Merck Co., (Germany). Methanol with high performance liquid chromatography (HPLC) grade was also acquired from Merck Co. Water with HPLC grade was supplied by Samchum Company (South Korea). Additionally, deionized water was employed in performing the experiments and supplying the solutions.

### 2.2. MNPs provisions and features

The co-precipitation method was applied in synthesizing MNPs. In this regard, 40.0 mL of 0.25 M solution of  $Cu(NO_3)_2 \cdot H_2O$  and 40.0 mL of 0.50 M solution of  $Fe(NO_3)_3 \cdot 6H_2O$  were combined via a magnetic stirrer during 15 min. Then, the ammonia solution (25.0%) was dribbled into the combination. By addition of the ammonia, the pH of the solution was checked. When reaching 12.0–12.5, the pH induces a dark precipitate. The precipitates were heated at temperature 80°C for 1 h, and then, they were repeatedly rinsed by deionized water. Afterward, they were detached through an external magnet, and were dried up at temperature 105°C for 2 h. At the last stage, the acquired samples were calcinated at temperature 600°C for 4 h [35,36].

The morphology and particle size were studied via a field emission scanning electron microscopy (FESEM) (MIRA3 TESCAN, Czech Republic). A Fourier transform infrared (FTIR) spectra was applied to determine the bond group in MNPs recorded through a BRUKER TENSOR II (Germany). Crystallographic MNPs structure was specified by the X-ray diffraction (XRD) analysis registered using a D8 advanced Bruker diffractometer with Ka-Cu radiation (Germany). The Brunauer–Emmett–Teller (BET) specific surface area as well as pore volume were measured through the  $N_2$  adsorption/desorption with a Belsorp mini II Japan. The distribution of pore size was computed via the Barrett, Joyner, and Halenda (BJH) technique.

### 2.3. Degradation of DZN through KMPS/MNPs/ozone

A stock of DZN solution was daily established via dissolving DZN in 1 L deionized water by a magnetic stirrer intended for 30 min. Afterward, it was set on an ultra-sonic instrument for 30 min. A KMPS solution was daily set up by dissolving KMPS in 250 mL of deionized water. To arrange an ozone stock solution, an ozone generator of capacity 0.4 g/h was employed. The ozone gas was constantly sparged in the bottom of a 1 L reactor with 500 mL deionized water solution by a ceramic diffuser during 30 min leading to a steady state with ozone concentration as  $0.1584 \pm 0.01$  g/L. The concentration of ozone was always figured out by the iodometric method. At the outset (KMPS/MNPs/ozone), some amounts of KMPS and MNPs were supplemented to the DZN solution (5.0–40.0 mg/L) in a 100 mL sealed flask. A known aliquot of ozone stock solution was inserted to the solution to obtain the suitable aqueous ozone concentration (4.0–20.0 mg/L). The flask holding the solution was mixed

by a shaker subject to the conditions of 250 rpm and 25°C. The solution pH was adjusted by sulfuric acid and sodium hydroxide (0.1 M). Samples were obtained at regular intervals and filtered by a 0.22  $\mu$ m syringe filter for the DZN analysis. Then, the samples were quenched by ethanol.

### 2.4. Analytical procedures

DZN was determined by a HPLC (KNAUER, Germany) with an ultraviolet (UV) detector. The detection wavelength of DZN was 220 nm based on the results of the spectrophotometer scan. The stationary phase was run by applying a C-18 column (150 mm  $\times$  4.6 mm). The isocratic mobile phase was performed through a ratio of 70:30 of water and methanol with the flow rate of 0.8 mL/min. Additionally, 20  $\mu$ L of sample was manually injected, while the column temperature was maintained at 30°C. Retention time was 4.8–5.2 min for the DZN peak, while the analysis time was continued up to 10.0 min. The calibration curve *R*-squared was 0.9999 for nine levels of DZN (0.01–40.0 mg/L). Total organic carbon (TOC) was evaluated by a TOC analyzer (Shimadzu, Japan). Chemical oxygen demand (COD), biochemical oxygen demand (BOD), bicarbonate, chloride, and sulfate ions were measured in accordance with standard methods [37]. TDS was evaluated via a TDS meter (HACH, Germany). The concentrations of copper and iron were specified through an atomic absorption spectrometer (AA spectrophotometer CTA-3000).

### 2.5. Gas chromatography–mass spectroscopy analysis

Gas chromatography–mass spectroscopy (GC/MS) analysis was employed to prepare the intermediates of DZN degradation using GC (7890B, Agilent, USA) equipped with a mass spectrometer (5977B, Agilent, USA). A capillary column (VF-1 ms, 15 m, 0.25 mm, and 0.25  $\mu$ m) was used in the analysis. Helium served as the carrier gas, and the samples were analyzed under the following conditions: initial temperature at 39°C for 4 min, ramp up at 8°C/min to 80°C and remained for 1 min, ramp up at 10°C/min to 150°C and remained for 1 min, then increased to 260°C with a ramp up of 10°C/min, injector = 80°C, volume = 5.0  $\mu$ L, split = 20, source temperature = 250°C, and full scan. Compounds were recognized via comparing their respective mass spectra and relative abundance of acceptance match criteria to those of standards, and through comparing them to the pesticide, NIST, and Wiley mass spectral library.

### 2.6. Measurement of ozone in solution

To measure ozone, we resorted to iodometry [38]. The ozone dosage was determined by the titration iodometric method, which is run semi-intermittently, and in which ozone is measured by adding gas ozone to the discontinuous reactor. It depends on the mass transfer characteristics of the reactor. Moreover, some compounds that consume ozone may evaporate during the examination.

### 2.7. Required chemicals

Sulfuric acid 2 normal, standard solution of sodium thiosulfate 0.01 normal, standard solution of sodium thiosulfate 0.05 normal, and iodide potassium solution 2%.

### 2.8. Experiment method

The ozone output from the generator was determined by passing the ozone gas through distilled water solution. The 200 mL container with the addition of 2% potassium iodide solution was acidified with sulfuric acid. Then, it was titrated by thiosulfate 0.005 or 0.01 normal. Following disappearance of the yellow color of the solution, 2–4 mL starch reagent solution was added, and titration continued until the blue color disappeared. Finally, the value of ozone was obtained via the following relation:

$$\text{Ozone (mg/L)} = \frac{(A - B) \times N \times 24}{V} \quad (4)$$

In Eq. (4),  $A$  (mL) represents the thiosulphate sodium consumed in the sample container,  $B$  (mL) is the thiosulphate sodium consumed in the control container,  $N$  stands for the normality of thiosulfate, and  $V$  (L) designates the volume of the sample.

### 2.9. Determination of zero load point

In this research,  $\text{pH}_{\text{zpc}}$  of copper nanoferrite was determined using the pH alteration method. To this end, 30 mL potassium nitrate 0.1 molar (electrolyte) was poured into six 50 mL bechers, and the pH of each solution was regulated using potassium hydroxide and nitric acid 0.01 molar in the range 2–12. Each Becher was added by 0.5 g copper nanoferrite. Magnet was used to stir the solution. The opening of the bechers was blocked by parafilm to prevent evaporation of the solution and entry of atmospheric gases. The bechers were put on a shaker for 48 h at 120 rpm. After the lapse of the required time, the pH of each solution was read by a pH-meter. At the last stage, the initial values of pH were drawn vs. the differences of initial pHs, and  $\text{pH}_{\text{zpc}}$  was recognized from its intersection with the zero point equal to 7 [38].

## 3. Results and discussions

### 3.1. MNPs attributes

Fig. 1a shows the FESEM of the synthesized MNPs. FESEM is used to characterize the size and morphology of the nanoparticles. As seen, the copper ferrite nanoparticles are sphere-shaped and arranged side by side with relatively the same sizes. The average sizes of these nanoparticles fall in the interval 19–27 nm. In addition, the agglomeration of nanoparticles may occur owing to their magnetic properties as well as interactions [39,40].

$\text{N}_2$  adsorption/desorption was applied to determine the pore diameters and surface area of the nanoparticles. Fig. 1b<sub>1</sub> depicts the  $\text{N}_2$  adsorption/desorption diagram for MNPs, and it portrays the pore diameter distribution (Fig. 1b<sub>2</sub>). Accordingly, the surface area of MNPs was obtained as 36/323 m<sup>2</sup>/g. The average diameter of the nanoparticles was, according to Fig. 1b<sub>1</sub>, estimated as 17/593 nm, while the pore volume was obtained as 0.1598 cm<sup>3</sup>/g. Based on the results, the synthesized nanoparticles are set in the mesopore category, and hence have an

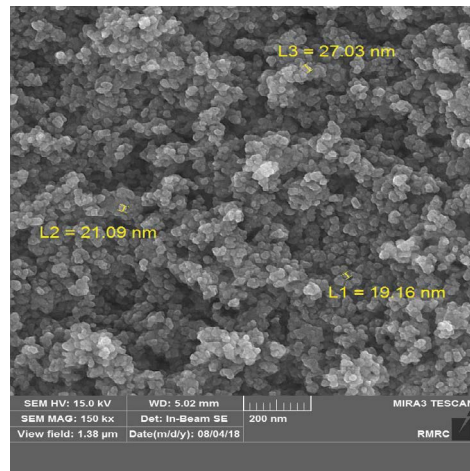
appropriate catalytic capacity. Fig. 1c shows the M-H hysteresis for MNPs. At the presence of a magnet, the MNPs could be easily recovered, which may be considered a good synthesis [31,41]. Fig. 1d shows the EDS spectra of MNPs where the inadequacy of impurity in the prepared MNPs is observed in consideration of the peaks of Fe, Cu, and O. Weight percentages of Fe and Cu were regarded as 21%/28% and 28%/4%, respectively, which in view of the  $\text{CuFe}_2\text{O}_4$  structure, is in harmony with the latter synthesis.

Fig. 1e illustrates the XRD spectra of the synthesized MNPs used in determination of the crystal phase. The diffraction peaks at the angles  $2\theta = 18.43^\circ, 30.35^\circ, 35.75^\circ, 43.35^\circ, 57.25^\circ,$  and  $62.92^\circ$  correspond to the levels (111), (220), (311), (400), (511), and (440), respectively. All these levels are consistent with (JCPDS file no. 77-0010) and are an evidence of the crystal structure of  $\text{CuFe}_2\text{O}_4$ . The results indicate the lack of impurity of the synthesized  $\text{CuFe}_2\text{O}_4$ . Fig. 1f illustrates the FTIR spectra of the MNPs. As observed, two sharp vibrations are occurred at 432.96 and 524.5 cm<sup>-1</sup>, which may be pertained to the bands of Fe–O and Cu–O in the MNPs. Various analyses conducted with the aim of determining the features of MNPs had results showing that the synthesized nano-particle had magnetic properties with high purity in both mesopore and nano contexts.

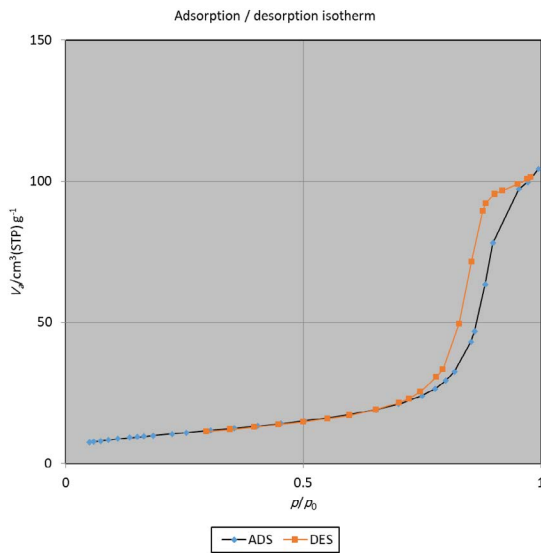
### 3.2. Impacts of effective factors

The pH of solution is reckoned amongst the effective parameters in AOPs. In addition to influence of the oxidizing power of radicals, pH may concern the catalyst's surface, and expedite the effect of adsorption of pollutants and oxidant upon the catalyst [42]. To this end, the competence of DZN removal was studied under the conditions of ozone concentration = 6 mg/L, catalyst dose = 0.1 g/L, KMPS = 0.6 g/L, and DZN concentration as 20 mg/L during a 20 min experiment time with the results presented in Fig. 2a. According to these results, the high efficiency was observed around neuter pHs and above, so that the proficiency of DZN degradations in the pHs: 3, 4, 5, 6, 7, 8, 9, and 10 were obtained as 87%, 94%, 95.3%, 97.5%, 99.2%, 99.3%, 99.3%, and 99.5%, respectively. In fact, the efficiency of the process has been reduced under acidic conditions. The high competence in neuter and alkaline situations may be because the alkaline conditions of degradation in the ozonation progress toward generating free radicals; however, KMPS moves non-radically in such conditions [43,44]. It should be noted that the oxidation power of radicals, particularly hydroxyl radical, and diminishes in alkaline pHs. Therefore, the oxidation power as for the hydroxyl radical is 1.8 V in alkaline pHs, and is equal to 2.8 V in acidic conditions [11]. Furthermore, the value of  $\text{pH}_{\text{zpc}}$  of the synthesized catalyst was obtained as 7. In other words, the efficiency of the process in high pHs does not increase owing to this issue. In addition, the catalyst surface receives a negative charge under alkaline conditions ( $\text{pH} > 7$ ), and repulsion occurs between the catalyst and peroxy monosulfate as an oxidant. Moreover, the electrostatic repulsion may occur between the catalyst and the negative charges of diazinon.

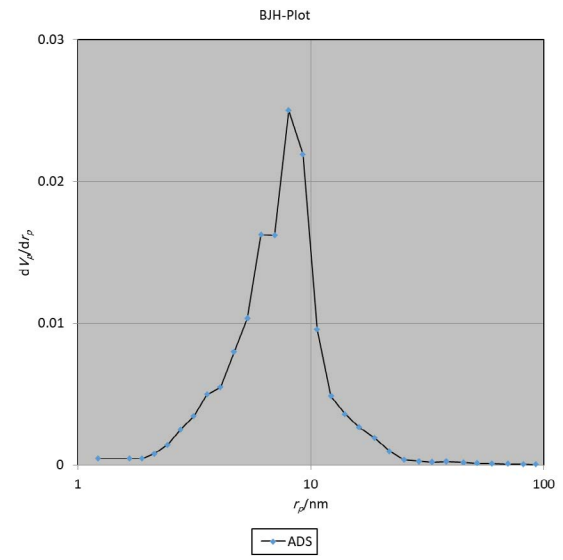
Most investigations on sulfate radical processes indicated that the proper action of the system occurred under neutral conditions. It is observed that the efficiency of the process



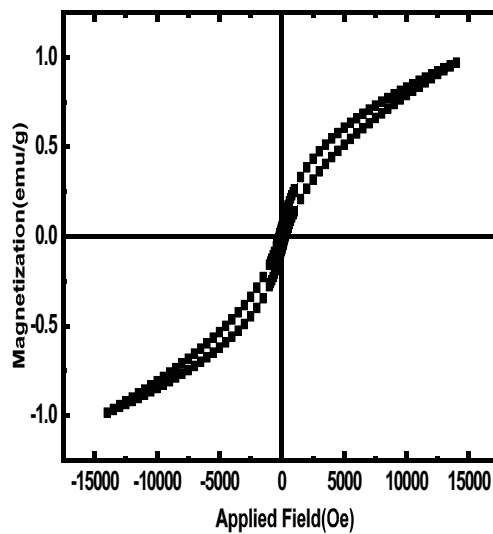
(a) FESEM image



(b<sub>1</sub>) Nitrogen adsorption–desorption isotherm

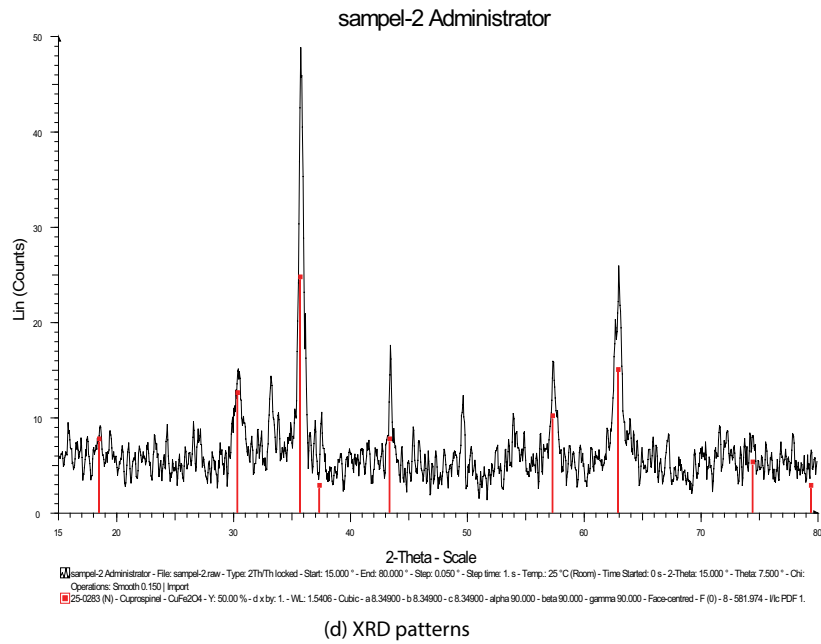


(b<sub>2</sub>) Pore size distribution (inset)

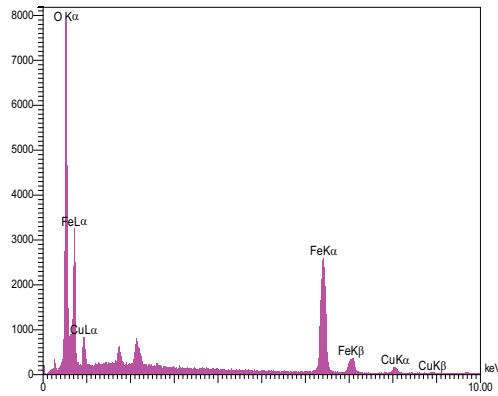


(c) Magnetization (M) vs. applied magnetic field (H)

Fig. 1. Features of  $\text{CuFe}_2\text{O}_4$  (a) FESEM image, (b<sub>1</sub>) nitrogen adsorption–desorption isotherm, (b<sub>2</sub>) pore size distribution (inset), and (c) magnetization (M) vs. applied magnetic field (H).



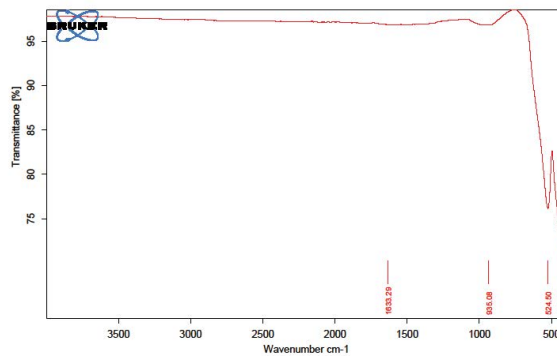
(d) XRD patterns



(e<sub>1</sub>) EDS spectra

Elt	Line	Int	Error	K	Kr	W%	A%	ZAF	Formula	Ox%	Pk/Bg	Class	LConf	HConf	Cat#
O	Ka	655.1	17.5657	0.4834	0.3004	50.25	78.81	0.5977		0.00	175.01	A	49.53	50.97	0.00
Fe	Ka	648.9	1.2924	0.4293	0.2667	28.47	12.79	0.9368		0.00	43.27	A	28.07	28.88	0.00
Cu	La	101.9	23.4677	0.0873	0.0542	21.28	8.40	0.2550		0.00	9.19	A	20.51	22.05	0.00
				1.0000	0.6213	100.00	100.00			0.00					0.00

(e<sub>2</sub>) EDS



(f) FTIR spectra.

Fig. 1. Features of CuFe<sub>2</sub>O<sub>4</sub> (d) XRD patterns (e<sub>1</sub> and e<sub>2</sub>) EDS spectra and (f) FTIR spectra.

was also reduced under acidic conditions, which may be due to the attendance of overload proton ( $H^+$ ) capable of scavenging oxidizing agents of hydroxyl and sulfate radicals (reactions (5) and (6)) [45,46]. This phenomenon occurs in most studies to degrade a dyestuff and the resistant organic materials in processes based on sulfate and hydroxyl radicals [45,47]. Consistent with the results, pH = 7 was adopted. Table 1 presents the statistical results of this section:



The oxidant dosage as the major agent has always been directly associated with the generation of free radicals. Thus, the effects of ozone concentration were examined

Table 1  
Statistical results of pH optimization

		Descriptive		Statistics	Standard error
pH optimum	Mean			6.50	0.866
	95% confidence interval for mean	Lower bound		4.45	
		Upper bound		8.55	
	5% trimmed mean			6.50	
	Median			6.50	
	Variance			6.000	
	Standard deviation			2.449	
	Minimum			3	
	Maximum			10	
	Range			7	
	Interquartile range			5	
	Skewness			0.000	0.752
	Kurtosis			-1.200	1.481
	pH optimum	Mean			0.42813
95% confidence interval for mean		Lower bound		0.06874	
		Upper bound		0.78751	
5% trimmed mean				0.40903	
Median				0.26250	
Variance				0.185	
Standard deviation				0.429877	
Minimum				0.000	
Maximum				1.200	
Range				1.200	
Interquartile range				0.700	
Skewness				1.042	0.752
Kurtosis				-0.146	1.481
pH optimum		Mean			97.8575
	95% confidence interval for mean	Lower bound		96.0618	
		Upper bound		99.6532	
	5% trimmed mean			97.9528	
	Median			98.6850	
	Variance			4.614	
	Standard deviation			2.14794	
	Minimum			94.00	
	Maximum			100.00	
	Range			6.00	
	Interquartile range			3.49	
	Skewness			-1.043	0.752
	Kurtosis			-0.143	1.481

under the conditions pH = 7, catalyst dosage = 0.1 g/L, KMPS = 0.6 g/L, DZN concentration as 20 mg/L during 20 min with the results shown in Fig. 2b. As the ozone concentration grows, the proficiency of the process slightly increases as expected, which may correspond to more creation of free radicals and reactive oxygen species (ROS). Once the ozone concentration was zero, the efficiency of the KMPS/copper nanoferrite system reached 95.3%, which may be linked to the generation of sulfate radical owing to the activation of KMPS by copper nanoferrite. By adding ozone dosage, the efficiency of the process was slightly increased guaranteeing that the presence of ozone raises the free radical generation. However, no significant effects were observed by the furtherance of ozone concentration. This is due to the reaction of ozone with hydroxyle and sulfate radicals, so that the less oxidizing radicals of hydroperoxyle and KMPS were produced. The overdosing of the ozone concentration in sulfate radical-based processes has not been yet tested. Nevertheless, the ozone overdosing is reported in both catalyzer and direct ozonation processes [48,49]:



Accordingly, an 8 mg/L concentration could justify the liability of ozone concentration in the system. Table 2 presents the statistical results of this section.

Moreover, the KMPS concentration may contribute to production of oxidizing species. The effect of KMPS dosage on the conditions of pH = 7, catalyst dosage of 0.1 g/L, 6 mg/L of ozone, and DZN concentration of 20 mg/L was studied in 20 min experiment. Fig. 2c shows the results. In the absence of KMPS (ozone/copper nanoferrite), the efficiency of DZN removal reached 87% due to the catalytic degradation of ozone in the catalyst surface. Addition of 0.3 g/L of KMPS caused to enhance the efficiency of producing free radicals. By increasing to 0.6 g/L, the process efficiency for the DZN removal reached 95.3%. No efficiency boost was attained by increasing the KMPS dosage to 0.6 g/L. This is the result of the reaction of free radicals with the excess or non-reacted KMPS, not with DZN [14,50].

Many researchers have investigated the scavenging effect of KMPS on high concentrations. Jaafarzadeh et al. [16] reported such a considerable effect in the case of dye removal. Additionally, in 2009 [51], this fact was accompanied by the indication that the reaction speed of KMPS with these radicals was very high ( $10^5/\text{M s}$ ) [51,52]. To provide active sites for the degradation of oxidants, the catalyst dosage well affects the activation of the latter. In this regard,

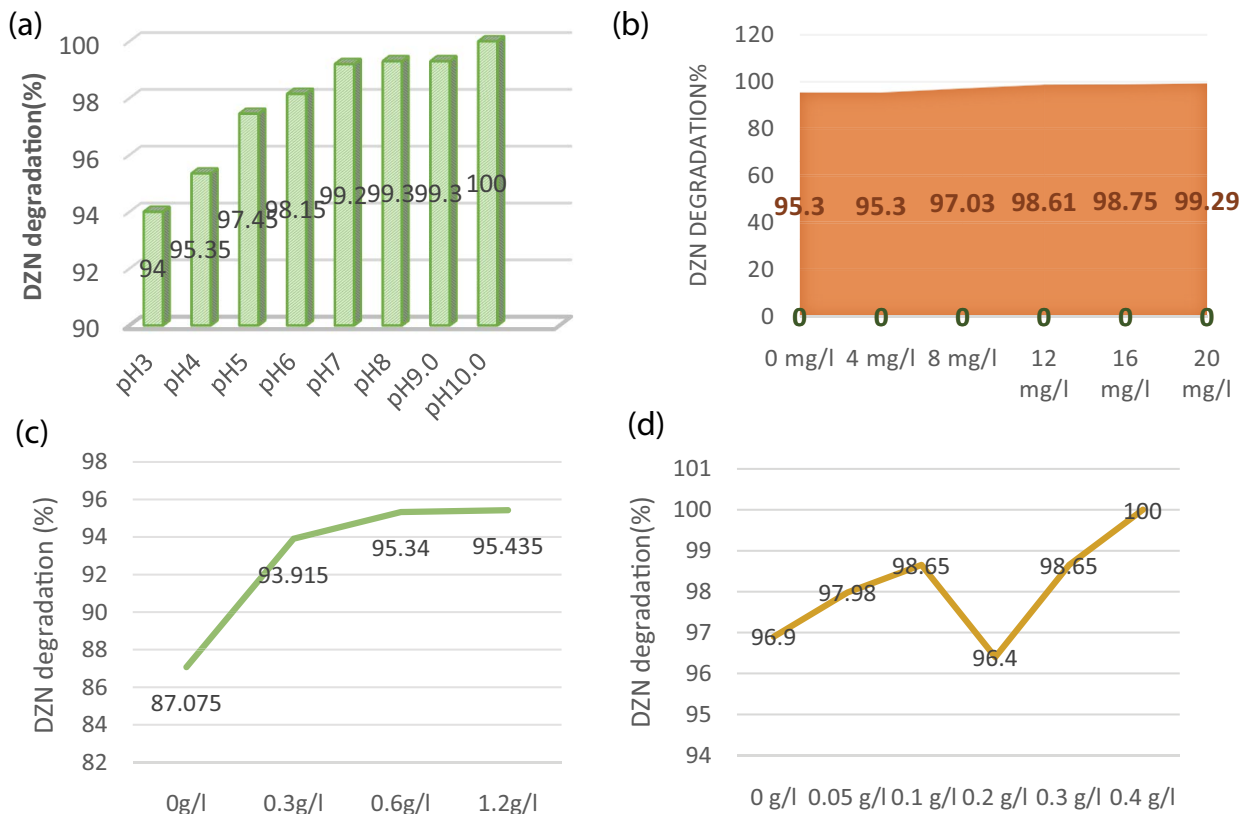


Fig. 2. Effective parameters in the KMPS/MNPs/ozone system for DZN elimination: (a) the impact of pH (20.0 mg/L DZN, 0.6 g/L KMPS, 6 mg/L  $\text{O}_3$ , 0.10 g/L MNPs, and 20 min reaction time), (b) the impact of ozone dosage (pH = 7.0, 0.6 g/L KMPS, 0.10 g/L MNPs, 20.0 mg/L DZN, and 20 min), (c) the influence of KMPS concentration (pH = 7.0, 6 mg/L  $\text{O}_3$ , 0.10 g/L MNPs, 20.0 mg/L DZN, and 20 min), and (d) the impact of MNPs loading (pH = 7.0, 6 mg/L  $\text{O}_3$ , 0.6 g/L KMPS, 20.0 mg/L DZN, and 20 min).

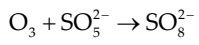
Table 2  
Statistical results of the optimizing ozone

		Descriptive		Statistics	Standard error
Ozone optimum	Mean			10.00	3.055
	95% confidence interval for mean	Lower bound		2.15	
		Upper bound		17.85	
	5% trimmed mean			10.00	
	Median			10.00	
	Variance			56.000	
	Standard deviation			7.483	
	Minimum			0	
	Maximum			20	
	Range			20	
	Interquartile range			14	
	Skewness			0.000	0.845
	Kurtosis			-1.200	1.741
	Ozone optimum	Mean			0.52067
95% confidence interval for mean		Lower bound		0.15140	
		Upper bound		0.88993	
5% trimmed mean				0.51846	
Median				0.43550	
Variance				0.124	
Standard deviation				0.351871	
Minimum				0.141	
Maximum				0.940	
Range				0.799	
Interquartile range				0.704	
Skewness				0.343	0.845
Kurtosis				-2.297	1.741
Ozone optimum		Mean			97.3950
	95% Confidence interval for mean	Lower bound		95.5505	
		Upper bound		99.2395	
	5% trimmed mean			97.4061	
	Median			97.8200	
	Variance			3.089	
	Standard deviation			1.75759	
	Minimum			95.30	
	Maximum			99.29	
	Range			3.99	
	Interquartile range			3.52	
	Skewness			-0.344	0.845
	Kurtosis			-2.297	1.741

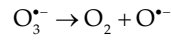
the catalyst dosage was studied under the conditions of pH = 7, 0.6 g/L of KMPS, 6 mg/L of ozone with 20 mg/L DZN during 20 min. Fig. 2d shows the results. As observed, in the absence of copper nanoferrite (ozone/KMPS), the process efficiency to remove DZN is 81.9%, indicating that the interplay between these two oxidants is more effective

than the ozonation and activation of the KMPS heterogen. Moreover, it demonstrates that ozone and KMPS have a synergic effect, so that ozone plays the role of an activator for KMPS. In fact, ozone first reacts with the ion of KMPS to generate ozonide and KMPS radicals. Then, during the following reactions, the sulfate and hydroxyle radicals will be degraded

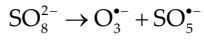
as the final product and the major agent of degradation [53].  
Table 3 presents the statistical results of this section:



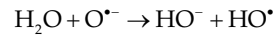
(9)



(13)



(10)



(14)



(11)

Adding nanoferrite to the system, the efficiency was increased, so that in dosages 0.5, 0.1, 0.2, 0.3, and 0.4 mg/L,

Table 3  
Statistical results of KMPS optimization

		Descriptive		Statistics	Standard error
KMPS optimum	Mean			0.875	0.4270
	95% confidence interval for mean	Lower bound		-0.484	
		Upper bound		2.234	
	5% trimmed mean			0.861	
	Median			0.750	
	Variance			0.729	
	Standard deviation			0.8539	
	Minimum			0.0	
	Maximum			2.0	
	Range			2.0	
	Interquartile range			1.6	
	Skewness			0.753	1.014
	Kurtosis			0.343	2.619
	KMPS optimum	Mean			1.41175
95% confidence interval for mean		Lower bound		0.14764	
		Upper bound		2.67586	
5% trimmed mean				1.37428	
Median				1.07450	
Variance				0.631	
Standard deviation				0.794430	
Minimum				0.913	
Maximum				2.585	
Range				1.672	
Interquartile range				1.325	
Skewness				1.826	1.014
Kurtosis				3.330	2.619
KMPS optimum		Mean			92.94125
	95% confidence interval for mean	Lower bound		86.62068	
		Upper bound		99.26182	
	5% trimmed mean			93.12861	
	Median			94.62750	
	Variance			15.778	
	Standard deviation			3.972148	
	Minimum			87.075	
	Maximum			95.435	
	Range			8.360	
	Interquartile range			6.626	
	Skewness			-1.826	1.014
	Kurtosis			3.330	2.619

the DZN removal efficiency was obtained as 95.9%, 98.6%, 96.4%, 98.6%, and 98.8%, respectively. One can observe that the efficiency increases with the increase of the catalyst concentration; however, no efficiency increase was occurred after a 0.1 mg/L increase. Therefore, even such a value of concentration may affect the system. Table 4 displays the statistical results of this section.

According to Table 5, Jaafarzadeh et al. [54] used the process of ozone/CuFe<sub>2</sub>O<sub>4</sub>/PMS to degrade 2,4-dichlorophenoxyacetic. The results of various experiments implied that this combination could degrade 2,4-dichlorophenoxyacetic under the conditions of pH = 6.0, 2.0 mM PMS, 16.0 mg/L O<sub>3</sub>, and 0.2 g/L catalyst. The nanoparticle CuFe<sub>2</sub>O<sub>4</sub> outshines its compounds, namely CuO and Fe<sub>2</sub>O<sub>3</sub>. It is a

Table 4  
Statistical results of MNPs optimization

		Descriptive	Statistics	Standard error	
MNPs optimum	Mean		1.6750	0.66254	
	95% confidence interval for mean	Lower bound	-0.0281		
		Upper bound	3.3781		
	5% trimmed mean		1.6389		
	Median		1.5000		
	Variance		2.634		
	Standard deviation		1.62288		
	Minimum		0.00		
	Maximum		4.00		
	Range		4.00		
	Interquartile range		3.21		
	Skewness		0.395		0.845
	Kurtosis		-1.470		1.741
	MNPs optimum	Mean			0.37850
95% confidence interval for mean		Lower bound	0.10646		
		Upper bound	0.65054		
5% trimmed mean			0.38100		
Median			0.33650		
Variance			0.067		
Standard deviation			0.259229		
Minimum			0.000		
Maximum			0.712		
Range			0.712		
Interquartile range			0.439		
Skewness			-0.106	0.845	
Kurtosis			-0.605	1.741	
MNPs optimum		Mean		98.1050	0.52918
	95% confidence interval for mean	Lower bound	96.7447		
		Upper bound	99.4653		
	5% trimmed mean		98.0922		
	Median		98.3150		
	Variance		1.680		
	Standard deviation		1.29622		
	Minimum		96.44		
	Maximum		100.00		
	Range		3.56		
	Interquartile range		2.20		
	Skewness		0.111	0.845	
	Kurtosis		-0.597	1.741	

Table 5  
Comparison of the catalyst dose to other references

Oxidation system	Catalyst	Catalyst dosage	Oxidizing	Reference
Ozone/CuFe <sub>2</sub> O <sub>4</sub> /PMS	CuFe <sub>2</sub> O <sub>4</sub>	0.2 g/L	2,4-dichlorophenoxyacetic	[54]
Alumina-supported Ni catalysts/ozone	Alumina-supported Ni catalysts	0.1 g/L	2,4-dichlorophenoxyacetic	[55]
Ozone/CuFe <sub>2</sub> O <sub>4</sub>	CuFe <sub>2</sub> O <sub>4</sub>	2 g/L	Phenacetin	[33]
Fe <sup>0</sup> nanoparticles supported by biochar	Fe <sup>0</sup> nanoparticles	0.33 g/L	2,4-dichlorophenoxyacetic	[56]
MnFe <sub>2</sub> O <sub>4</sub> /PMS	MnFe <sub>2</sub> O <sub>4</sub>	0.05 g/L	Organic pollutants	[57]
CuFe <sub>2</sub> O <sub>4</sub> /PMS	CuFe <sub>2</sub> O <sub>4</sub>	0.1 g/L	Iopromide	[30]
Cu–Fe–O/ozone	Cu–Fe–O	1 g/L	Dyestuff	[58]
Fe–Co/ZrO <sub>2</sub> /ozone	Fe–Co/ZrO <sub>2</sub>	2 g/L	2,4-dichlorophenoxyacetic	[59]
Co <sub>2</sub> O <sub>3</sub> /PMS	Co <sub>2</sub> O <sub>3</sub>	0.2 g/L	Phenol	[60]

stable catalyst and could be re-used up to 5 times for more experiments and degradation [54]. Rodriguez [55] applied the ozonation process to remove 2,4-dichlorophenoxyacetic from the aquatic environment. The catalyst alumina/nickel oxide adapted by them was able to activate the ozone by 0.1 g/L. They reported that the catalyst could create the active radical types on the surface. Moreover, one could mention the usability of this catalyst under neutral conditions. A noteworthy by-product that appeared in this study is Malic acid, which is an indication of the sufficient presence of hydroxyle radical in the environment [55]. To degrade Fenastine, Q, [33] used catalytic ozonation. The catalyst used in that research was CuFe<sub>2</sub>O<sub>4</sub> made of chemical precipitation. The conclusion was that in the simple ozonation, both ozone and hydroxyle radical were the main agents in the degradation of the pollutant. In addition, they deduced that the presence of the catalyst by 2 g/L could increase the process efficiency; however, the catalyst has not high efficiency alone. Ying et al. [56] employed bone charcoal and the nanoparticle of iron in the absorption and degradation of 2,4-dichlorophenoxyacetic. They inferred, by their investigation, that the complete degradation has occurred through 330 mg/L iron, 170 mg bone charcoal, and 10 mg/g 2,4-dichlorophenoxyacetic during 40 h.

Yao et al. [57] used MnFe<sub>2</sub>O<sub>4</sub> as a catalyst to activate PMS. The efficiency of using this catalyst by 0.05 g/L is much above that of manganese homogen solution. Furthermore, the magnetic separation of this catalyst is especially easy. They showed that the re-use of this catalyst up to 4 times has no effects on the process efficiency. In the activation procedure of PMS, to degrade iopromide as a resistant pollutant, Zhang et al. [30] used CuFe<sub>2</sub>O<sub>4</sub>. They realized that the latter is more effectual than CuO from the viewpoints of efficiency and stability. The efficiency of PMS/CuFe<sub>2</sub>O<sub>4</sub> under the conditions of 0.2 mM PMS, pH = 6, 1 μM iopromide concentration, and 0.1 g/L catalyst during 10 min was nearly 80%. Liu et al. [58] used the process ozone/Cu–Fe–O in the degradation of a dyestuff. The catalyst was the combination of copper oxide and copper ferrite. They studied the effects of parameters such as pH, catalyst dose, ozone dose, initial concentration of the dyestuff, and the experiment time. The outcome of their experiment indicated an appropriate function of the degradation

process, so that the rates of COD and dye removal during 60 min and under the conditions of pH = 6.8, 30 mg/L ozone, and 1 g/L catalyst concentration were 70% and 90%, respectively. The corresponding rates in the simple ozonation were obtained as 48% and 66%, respectively. Finally, they pointed out the properness of the above-mentioned catalyst from the viewpoints of stability and reusability.

Nie et al. [59] resorted to the catalytic ozonation and the Fe–Co/ZrO<sub>2</sub> catalyst to degrade 2,4-dichlorophenoxyacetic. Their observations yielded the result that the process above was suitable in the degradation of 2,4-dichlorophenoxyacetic, so that they could mineralize more than 60% of organic carbon by 2 g/L catalyst in a concentration of 10 mg/L 2,4-dichlorophenoxyacetic. This showed a 30% increase in efficiency compared to the simple ozonation process. To activate PMS, Shukla [60] utilized active cobalt/activated carbon as a catalyst, and investigated the activation rate upon phenol degradation. The results of their study indicated that the main oxide was Co<sub>2</sub>O<sub>3</sub>. Phenol was completely degraded by 0.2 g/L catalyst during 60 h, while the organic carbon reduction as the mineralizing index was obtained as 80%. The final deduction made by them was that the cobalt/carbon enjoyed good stability, and that the activation of PMS in the presence of this catalyst followed the first-rate kinetic. In the present study, the system of ozone/KMPS/MNPs can completely degrade diazinon under the conditions: 6 mg/L ozone, 0.6 g/L KMPS, 0.1 g/L copper nanoferrite, and pH = 7, during 20 min.

As observed, the catalyst dose is optimum relative to similar researches. It could be so deduced that there is a synergy and overlap between the two oxidants of ozone and KMPS and copper nanoferrite as the catalyst in the degradation of diazinon. The synergy is also discerned in the experiment time, so that the duration of 20 min is extremely appropriate and optimum as compared to other similar investigations. The presumption of pH = 7 appears to have high vitality in the synergy effect and successive feat of the experiment. Overall, the ultimate inference is that the AOP applied in this research was thriving in the degradation, mineralization, and detoxification of the toxic substance of diazinon.

The effect of the initial DZN concentration in ozone/copper nanoferrite/KMPS was investigated for the range

5–40 mg/L with pH = 7, 0.6 g/L of KMPS, 6 mg/L ozone, and 0.1 g of catalyst for the duration of 20 min with the results shown in Fig. 3a. As observed, degradation of DZN was completed in low concentration, but in 10, 20, and 40 mg/L after 20 min, some of the pollutant was remained. Obviously, more time was needed for complete degradation. Indeed, the rate of radicals generated in the system was constant, so that with an increase in the number of the molecules in the pollutant (which means the increase in concentration), a smaller amount of the material was subject to radicals attack. The first-order rate kinetic was exercised to determine the reaction degree of DZN degradation. Accordingly, the following equation was applied:

$$-\ln \frac{[\text{DZN}]_t}{[\text{DZN}]_0} = kt \quad (15)$$

Here,  $k$  denotes the first-order rate constant ( $\text{min}^{-1}$ ),  $t$  designates the reaction time (min),  $[\text{DZN}]_0$  is the initial concentration of DZN (mg/L), and  $[\text{DZN}]_t$  stands for the concentration at time  $t$ . Fig. 3b depicts the diagram  $\log[\text{DZN}]$  against  $t$ . The values of  $k$  in the ozone/copper nanoferrite/KMPS process for the concentrations 5, 10, 20, and 40 mg/L are 0.4143, 0.2019, 0.1841, and 0.1728  $\text{min}^{-1}$ , respectively. As observed, the speed of degradation of DZN at the concentration of 5 mg/L is three times as much

as that at the concentration of 40 mg/L. Most studies have indicated that the constant  $k$  decreases as the initial concentration increases. In addition, the half-life of the pollutant at concentrations 5, 10, 20, and 40 mg/L was calculated as 1.67, 3.43, 3.67, and 4.01 min, respectively. In other words, at concentrations less than 40 mg/L, 50% of DZN is degraded in less than 5 min. These facts, along with the diagram above confirm that the degradation have well-followed the first-rate kinetic. The effect of temperature at 10°C, 25°C, and 45°C was examined under the conditions of pH = 7, 0.6 g/L of KMPS, 6 mg/L of ozone, concentration of 20 mg/L of DZN, and 0.1 g/L copper nanoferrite, and their reaction constant were presented in Fig. 3c. Decreasing temperature to 10°C led to dwindling of the constant  $k$ , which may be due to the deactivation of KMPS at low temperature. Several investigations have indicated that KMPS was not easily activated at temperature of 10°C. Furthermore, the increase in temperature caused a growth in  $k$  values. At high temperatures, KMPS were activated, the O–O bond was broken, and the hydroxyle and sulfate radicals were produced [61,62]. On the contrary, ozone became instable at high temperatures, and its solubility was decreased with a reduction of tendency to reaction with the catalyst and KMPS. Indeed, temperature had a dual effect upon the reaction, so that it increased or decreased the reaction speed [63,64]. One could express the changes of rate constant  $k$  with the temperature using the Arrhenius equation (Eqs. (16) and (17)).

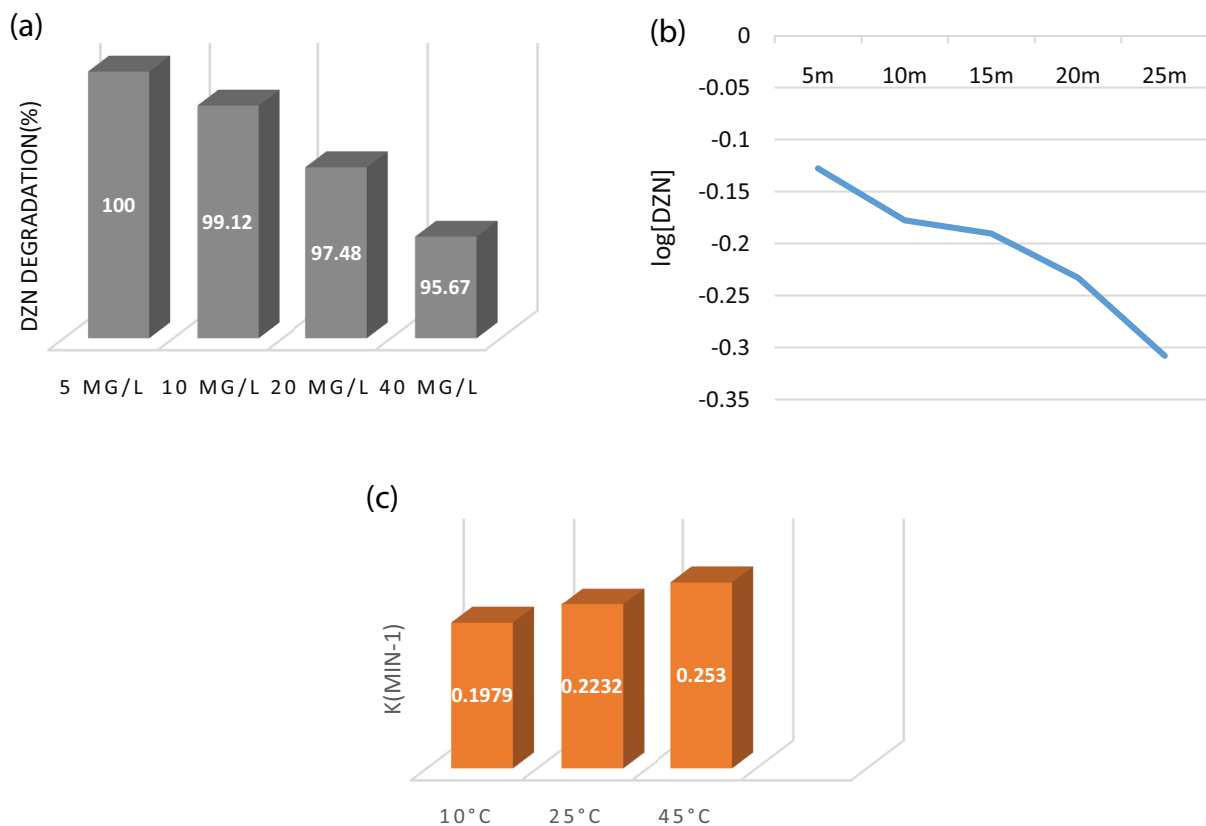


Fig. 3. (a) Impact of the initial DZN concentration on DZN degradation in KMPS/MNPs/ozone (pH = 7.0, 6 mg/L  $\text{O}_3$ , 0.6 g/L KMPS, and 0.10 g/L MNPs), (b)  $\log[\text{DZN}]$  against different times, (c) the rate constant of the first-order kinetic model at different temperatures (pH = 7.0, 7 mg/L  $\text{O}_3$ , 0.6 g/L KMPS, 0.10 g/L MNPs, and 20.0 mg/L DZN).

$$k = Ae^{-E_a/RT} \quad (16)$$

$$\log k = \log A - \frac{E_a}{2.303RT} \quad (17)$$

where  $A$  is the Eigen-constant of the reaction,  $e$  is the base of the natural logarithm,  $E_a$  is the activation energy (in J/mol),  $R$  denotes the mole gas constant, and finally  $T$  stands for the Kelvin temperature. The  $E_a$  value may be obtained from the rate constants at two different temperatures. Assuming that  $K_1$  is the rate constant at temperature  $T_1$ , and  $K_2$  is that at temperature  $T_2$ , then:

$$E_a = 2.303 \left( \frac{T_1 T_2}{T_2 - T_1} \right) \log \left( \frac{K_2}{K_1} \right) \quad (18)$$

where  $E_a$  for two temperatures 10°C and 25°C was obtained as 5.63 kJ/mol.

### 3.3. Reusability and stability

Possibility of reuse is reckoned among the applied aspects of the catalyst. As cited in the previous section, after the end of the reaction, the catalyst was separated via a magnet. Afterward, it was washed with deionized water before being dried up at a temperature of 65°C to be reused. DZN removal was measured once with a catalyst participating in the reaction, and the next time with a catalyst having no reactions under the conditions of pH = 7, 0.6 g/L of KMPS, 6 mg/L of ozone, concentration of 20 mg/L of DZN, and 0.1 g/L copper nanoferrite. Fig. 4 presents the results. We observe that the degradation percentage has fallen from 99.2% to 98.4% for the former catalyst. This less than 1% decline indicates the catalyst stability [65]. Recycling of the catalyst was performed only by washing and drying at a 65°C temperature under moderate conditions. Hence, one acknowledges that the synthesized copper nanoferrite is much more stable and apt for reusability; an issue which is environmentally considerable. The rate of leaching of iron and copper after the employment of MNPs in the KMPS/MNPs/ozone system was studied with 0.141 mg/L leaching value for iron and 0.061 mg/L value for copper. No significant leaching was detected in the system, which is a token of high stability of the catalyst. Wang

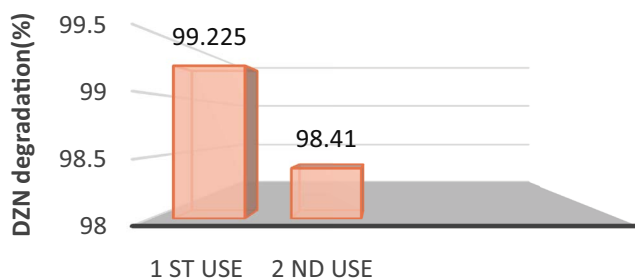
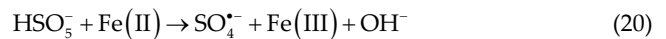
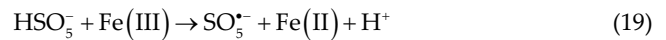


Fig. 4. Reuse of MNPs (pH = 7.0, 6.0 mg/L  $O_3$ , 0.6 g/L KMPS, 0.10 g/L MNPs, and 20.0 mg/L DZN).

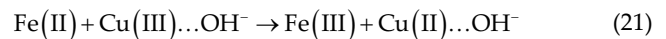
et al. [40] in their dye removal study demonstrated that while using only one oxidant, the leaching rate of the catalyst was more than 1 ppm. In another research using one oxidant, it was shown that the leaching rate was 0.1 mg/L [66].

### 3.4. Contrasts between processes evaluations

Catalytic systems were compared from the activity viewpoint. Under the conditions of pH = 7, 0.6 g/L of KMPS, 6 mg/L ozone, and 20 mg/L concentration of DZN in 20 min, and the results are presented in Fig. 7. In  $CuFe_2O_4$ , Cu(II) can make KMPS into sulfate radical and Cu(III). Furthermore, Cu(III) generates Cu(II) and  $SO_5^{\bullet-}$  when reacting with KMPS.  $SO_5^{\bullet-}$  in adjacency with each other could jointly generate sulfate radical and oxygen. Moreover, sulfate radical may be generated by the reaction of  $SO_5^{\bullet-}$  with ozone, affecting the DZN degradation [30,34]. Additionally, Fe(III) in the structure of  $CuFe_2O_4$  reacts with KMPS and produces  $SO_5^{\bullet-}$  and Fe(II). Then later, in turn, can generate sulfate radical [67,68].



In fact, the functions of both transition metals are effectual in the production of sulfate radicals. Since the standard potential of reduction of Cu(III)/Cu(II), Fe(III)/Fe(II), and  $HSO_5^-/HSO_4^-$  is 2.3, 0.77, and 1.82 V, Cu(III), respectively, which might be easily reduced via Fe(II) and KMPS [30].



The reduction/oxidation cycle of Fe(III)/Fe(II) and Cu(III)/Cu(II) has caused the synergic effect in copper nanoferrite. The catalyst operation when contacting with ozone is unlike KMPS, so that the radical generation is rendered by the hydroxyle groups bonded on the surfaces of metal oxides. Indeed, ozone is activated through the following chain reactions, and it has produced hydroxyle radicals [69,70].

### 3.5. Absorption differentiation and degradation reaction

According to investigations, persistent organic pollutants are not completely oxidized nor mineralized during the ozonation process. There are several ways to improve the oxidation capacity of organic compounds, which can reduce reaction time and the related costs. Accordingly, the combination of some catalysts with ozone has been widely considered for the treatment of industrial wastewater and surface water. The catalyst is regarded as a chemical compound that is able to exert an accelerating and directing effect on the progression of a reaction, which is thermodynamically possible [33,56].

Three mechanisms are identified in the non-homogeneous catalytic ozonation process, which are depicted in Fig. 5: (1) chemical absorption of ozone on the catalyst's surface causing to generate active varieties and oxidation of organic molecules; (2) chemical absorption of organic molecules on the catalyst's surface; (3) chemical absorption

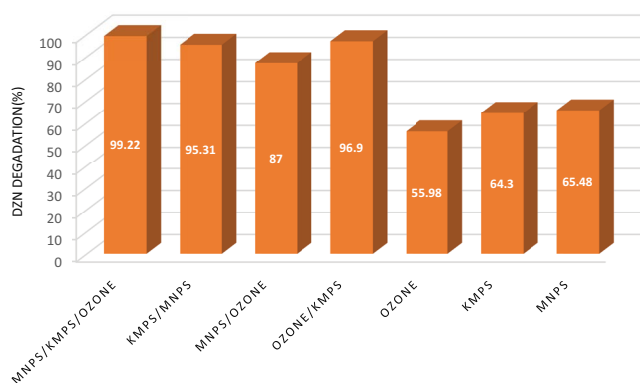


Fig. 5. Performance of different systems for DZN removal (DZN = 20 mg/L, KMPS = 0.6 g/L,  $O_3$  = 6 mg/L, MNPs = 0.1 g/L, pH = 7.0, and reaction time = 20 min).

of ozone and organic molecules on the catalyst's surface followed by the reaction of the absorbed varieties with each other [57,58].

The mere usage of oxidants (ozone and KMPS) and the catalyst, as observed, has not been of an ideal utility. Certain studies relate this to the catalyst dosage, not adsorption of DZN on the surface, low concentration of the oxidants, or their small potential in reaction with the pollutant. The column dedicated to MNPs shows the absorption of diazinon on the catalyst. In this stage, only absorption occurs at 65.48%, and since degradation does not occur, the nanoparticle cavities remain occupied by diazinon. In the MNPs/ozone; however, both diazinon and ozone are on the nanoparticles, and the absorption and degradation occur simultaneously and heterogeneously. Therefore, if this column is compared to the ozone column where diazinon is degraded homogeneously at 55.98%, one deduces that the presence of the nanoparticles as catalyst increases the efficiency of diazinon degradation by 31%. This efficiency increment is also observable in the column of KMPS/MNPs compared to that of KMPS. Finally, the synergy effect of absorption, along with degradation in the MNP<sub>s</sub>/KMPS/ozone system, is increased by 99.2%.

As Fig. 5 shows, if deionized water treatment is intended, the double KMPS/MNPs system can be used. However, if the water contains salts and organic matter like secondary effluent, the efficiency of the double system is diminished (Fig. 8c); to increase the efficiency, the triple system MNPs/KMPS/ozone must be chosen.

### 3.6. Effect of anions and natural water

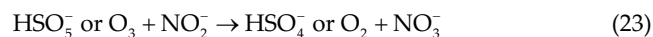
In water resources, the corporation of various compounds, particularly anions, may be influential on AOPs. Hence, the ozone/MNPs/KMPS process was studied in the presence of the existing anions, and the pertaining results are depicted in Fig. 6a. As seen, in the presence of sulfate ion, no significant changes were observed in the efficiency of the main process, which may be on account of the sulfate radical essence of the process. The effect of chloride ion on AOPs has been reported as inhibitory and promotional in the literature. Hereby, the generated radicals can be

scavenged and produce different species of chlorine ( $Cl^{\bullet}$ ,  $Cl_2^{\bullet-}$ ,  $ClOH^{\bullet-}$ , and  $Cl_2$ ), which has lower redox potential [71,72].

In addition, chloride ion may react directly with ozone and KMPS to inhibit the production of free radicals [24,73]. In this regard, Zhou et al. [74] investigated the impact of chloride ion concentration on orange II decolorization through KMPS/ $Co^{2+}$ . Chloride ion enjoyed a dual effect in the KMPS/ $Co^{2+}$  system, and contributed to removal efficiency plunge at low concentration (5 mM). Meanwhile, a high concentration of chloride ion (500 mM) has increased the rate constant by 4–15 fold [74,75]. In the present work, the efficiency of the process is found to be increased in the presence of chloride ion. Nitrate has low inhibitory effects, which may be arisen from the production of nitrate radicals with lower redox potential. In any case, these effects are not as much discernible as other anions. As for nitrite and bi-carbonate, the inhibitory effect was detected. Being a reductive material, nitrite is used in the scavenging of AOPs. Therefore, it is well-expected that in the presence of which, the system efficiency declines. The electron transfer mechanism throughout radical scavenging for nitrite is presented in the following reaction:



Nitrite could go alone into reaction with ozone and KMPS and deactivate them. Differently regarded as a strong reductive agent, nitrite may affect radicals and oxidants negatively [76].



Bicarbonate and carbonate are considered the most known scavengers of free radicals. As observed, the process efficiency is extremely decreased in the presence of bicarbonate, which is due to generation of carbonate and bicarbonate resulted from their reaction with free radicals. The radicals of carbonate and bicarbonate have 1.78 V redox potential, being much lower than that of sulfate and hydroxyl radicals. Moreover, the speed of reaction of bicarbonate and carbonate with organic compounds is 2–3 times lower than that of hydroxyl and sulfate [71,77,78]. Regarding phosphate, it could be mentioned, as pointed out in several references, that its direct reaction with ozone could yield the inhibitory effect. It is noteworthy that phosphate could bind with the catalyst surface, and was able to deactivate the oxidants. This deactivation property of phosphate is much greater than its scavenging property for radicals [79,80]. The presence of all anions in the system caused a slight decline in the process efficiency. In addition to what mentioned above, the decline might be due to increased ion strength. In other words, the ion strength increases with anions' concentration growth, leading to the impediment of radical generation. Fig. 6b presents the results of the ozone/MNPs/KMPS process in natural water.

DZN solution was injected into two real environments (tap water of Shiraz and secondary effluent of wastewater treatment plant of Shiraz). The system efficiency for the deionized water was 99.2%, which was used in the control experiment. The efficiency rates for tap water and

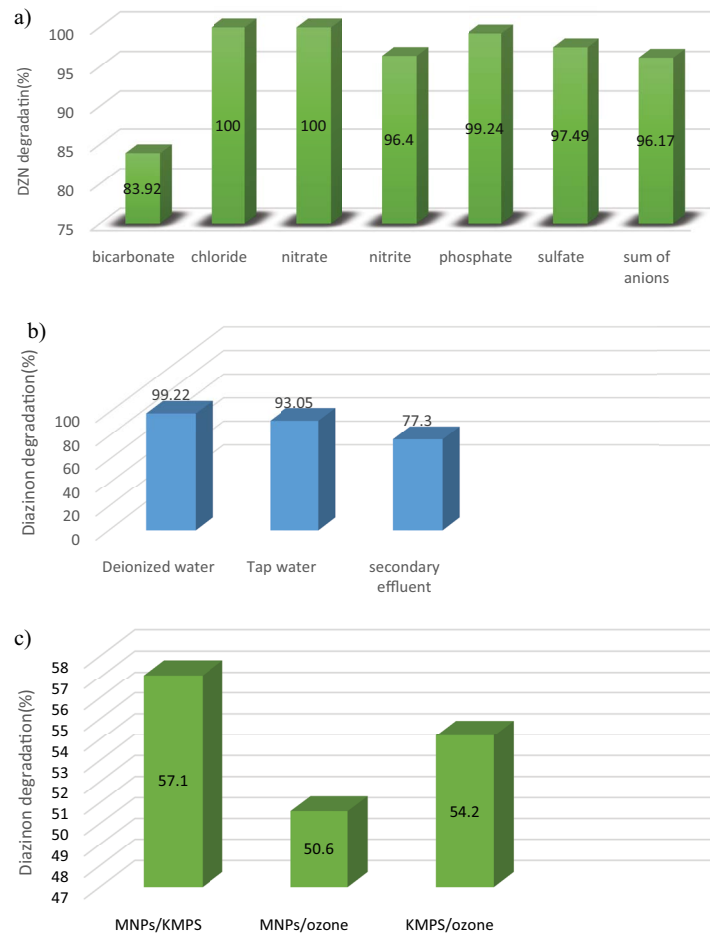


Fig. 6. (a) Influence of different anions on the DZN elimination (DZN = 20.0 mg/L, KMPs = 0.6 g/L,  $O_3$  = 6.0 mg/L, the catalyst = 0.10 g/L, pH = 7.0, and anion concentration = 3.0 mM), (b) the performance of the KMPs/MNPs/ozone in different matrices (DZN = 20.0 mg/L, KMPs = 0.6 g/L,  $O_3$  = 6.0 mg/L, the catalyst = 0.10 g/L, pH = 7.0, and reaction time = 20 min), and (c) binary systems performance in the diazinon degradation from secondary effluent (DZN = 20.0 mg/L, KMPs = 0.6 g/L,  $O_3$  = 6.0 mg/L, the catalyst = 0.10 g/L, pH = 7.0, and reaction time = 20 min).

secondary effluent were decreased to 93% and 77.3%, respectively. The slight decrement in tap water could be linked to the dissolved solids in water, which was elucidated above. The efficiency decrease of the process for the secondary effluent was much more than that for tap water. Coupled with different anions scavenging free radicals, the organic load content ( $BOD_5 = 70$  mg/L for secondary effluent) led the efficiency to 77.3%. This is because the organic materials existing in the secondary effluent emulate with DZN to react with radicals. Therefore, the reaction of free radicals with the target pollutant is stopped.

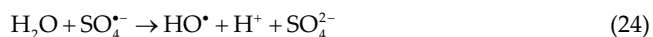
### 3.7. Active agents in DZN degradation

To identify active species in the degradation of pollutants, chemical alcohols are frequently used in sulfate radical-based processes. Accordingly, alcohol is employed to scavenge both hydroxyl and sulfate radicals, and another alcohol is used in the scavenging of the hydroxyl radical. The difference between these two scavengers shows

the contribution rate of the sulfate radical. In the present study, owing to high rate in reaction, we used ethanol to scavenge sulfate and hydroxyl radicals [81]. In additionally, alcohol without alpha hydrogen like *tert*-butyl alcohol (TBA) with  $k = 1/M s 8-7.6 \times 10^8$  was used to scavenge the hydroxyl radical.

The reaction speed of this alcohol is 1,000 times slower than that of the sulfate radical. Therefore, one can realize the contribution rate of hydroxyl and sulfate from the difference between them [82]. Hence, two scavengers of ethanol and TBA were analyzed in four systems to determine active species. These systems include ozone/MNPs/KMPs, ozone/MNPs, KMPs/MNPs, and ozone/KMPs. Fig. 7a depicts the effect of inhibitory factors on the ozone/MNPs/KMPs system. Ethanol has caused the system efficiency to decrease only to 27%, indicating the contribution of sulfate and hydroxyl radicals to DZN degradation. We observe that in the presence of TBA, the degradation rate has reached 65% for the duration of 20 min. This rate shows that the hydroxyl radical has played a minor role in

this phenomenon in respect to sulfate. Sulfate radical in the aqueous solution can be converted to the hydroxyl radical, which is pointed out by many authors like [57,83,84]:



In Fig. 7b, the system of ozone/KMPS follows almost the same procedure. Fig. 7c shows the effect of scavengers on the KMPS/copper nanoferrite system. In this Fig. 7, we observe that the degradation rate is decreased in the presence of the two scavengers of TBA and ethanol. This occurrence indicates that the main agents in the system are the hydroxyl and sulfate radical. Decreases in the values of removal efficiency are observable, demonstrating that the hydroxyl radical is responsible in the degradation. As stated before, in the water solution, the sulfate radical may be transformed into the hydroxyl radical. Fig. 7d illustrates the functions of the two scavengers in the ozone/copper nanoferrite. We observe that the conduct of ethanol is more distinguished than TBA, which is due to the highlighted role of the sulfate radical. Nonetheless, TBA is also accountable for the decline of the process efficiency. Specifically, it is the evidence for the performance of the hydroxyl radical in this system. From the above discussion, one infers that both active species in this system are fully responsible for the degradation.

### 3.8. Mineralization process

Mineralization of the process was studied in the ozone/MNPs/KMPS system based on the parameter TOC with the results presented in Fig. 8. As expected, the mineralization had a good rate of 61.9% in the TOC removal. This rate may occur due to the synergic effect of ozone, nano-particle, and KMPS. In fact, the generation of free radicals for mineralization in this system was sufficient.

### 3.9. Determination of by-products obtained from the DZN degradation by the ozone/MNPs/KMPS process

GC/MS analysis was applied to determine by-products in the process. As can be seen, six compounds of the

GC/MS spectrum were identified (Fig. 9). The pathway for the DZN degradation was proposed based on the obtained compounds. (It is worth mentioning that dichloromethane was used to extract DZN from water prior to the GC/MS analysis. For this reason, chlorine was set on some compounds resulted from the analysis, which were avoided in the proposal of the degradation pathway).

## 4. Conclusion

In this study, the process of ozone/MNPs/KMPS on the degradation of DZN – a high usage pesticide – was evaluated. According to the derived results, the ozone/MNPs/KMPS system can degrade completely 20 mg/L of diazinon under the conditions of 6 mg/L ozone, 0.6 g/L KMPS, 0.1 g/L MNPs, and pH = 7 during 20 min. The results demonstrated that the efficiency of the system was more related to the concentration of KMPS and nano-particle than to ozone. Therefore, the usage of KMPS and nano-particle in high concentration has not positive effects on the DZN degradation. Furthermore, the pH of the solution had a slight influence on the system, so that the efficiency had the highest rate in the range pH = 7–10. The pH in the range 3–6 showed no significant drop, and the DZN degradation

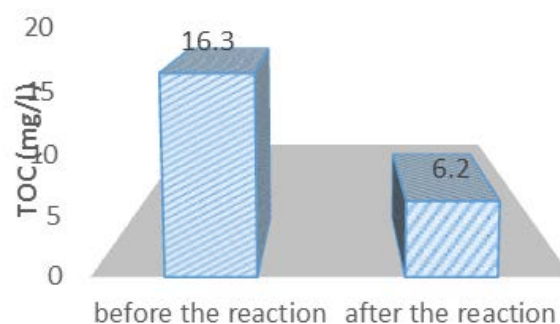


Fig. 8. TOC removal of (conditions: 20.0 mg/L DZN, pH = 7.0, KMPS = 0.6 g/L, O<sub>3</sub> = 6 mg/L, MNPs = 0.10 g/L, and 30 min).

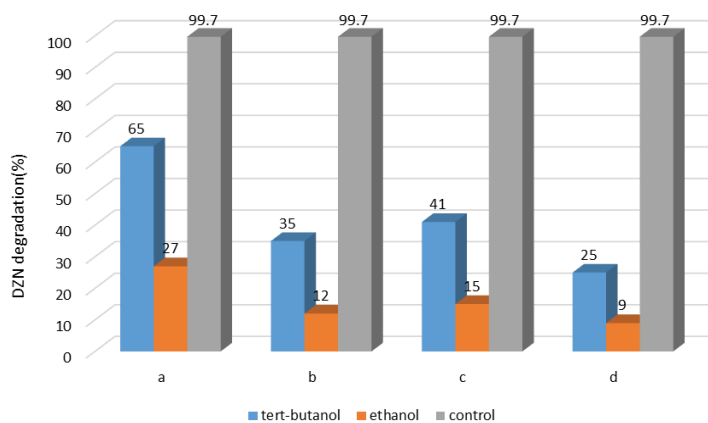


Fig. 7. Impacts of two scavenging agents on the DZN elimination (a) KMPS/MNPs/O<sub>3</sub>, (b) KMPS/O<sub>3</sub>, (c) KMPS/MNPs, and (d) MNPs/O<sub>3</sub> (conditions: pH = 7.0, KMPS = 0.6 g/L, O<sub>3</sub> = 6.0 mg/L, MNPs = 0.10 g/L, and TBA = ethanol = 11.5 g/L).

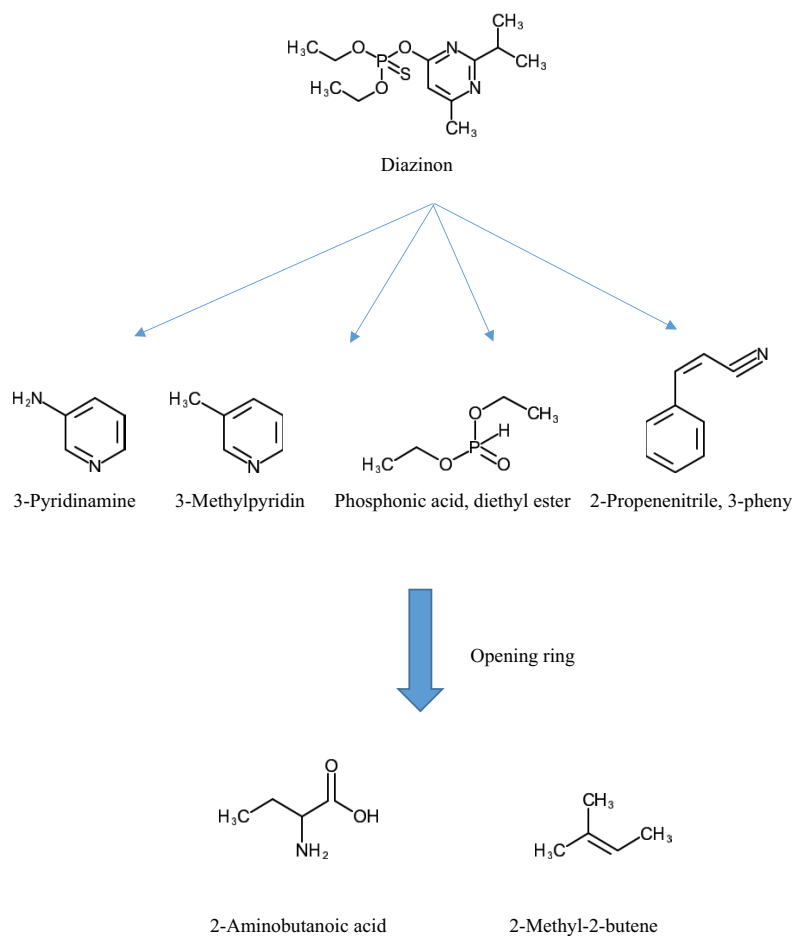


Fig. 9. Proposed pathway for the DZN degradation by ozone/CuFe<sub>2</sub>O<sub>4</sub>/KMPS (0.9 g/L KMPS, 8.0 mg/L O<sub>3</sub>, pH = 7.0, and 0.15 g/L MNPs, 25.0 mg/L DZN, and 60 min time of reaction).

was carried out with high percentage. A temperature above 25°C slightly affected the degradation. MNPs could be used in the system without losing its catalytic activity at the stage of reusability. Moreover, the leaching rate of iron and copper ions was inconsiderable. In the evaluation of the process in the presence of different anions, it was indicated that bicarbonate had the most, and nitrite had the least inhibition. The process efficiency was also scrutinized in several real waters. The active agents were recognized using the scavenging agents, and the contribution of hydroxyl and sulfate radicals in the DZN degradation was revealed. The by-products were analyzed using GC/MS, and 6 intermediate compounds were characterized before proposing the DZN oxidation. Eventually, a combination of AOPs in this work was capable of refining such a resistant pollutant as DZN in the water environment. Although any merger of processes complicates their mechanism and analysis, the current study promises the advent of hybrid processes in water and wastewater treatment.

## References

- [1] K.T. Jahromi, Pesticides Toxicology, 5th ed, University of Tehran Press, Tehran, Iran, 2013, pp. 407–500.
- [2] Y. Zang, K. Pagilla, Treatment of malathion pesticide waste water with nanofiltration and photo-Fenton oxidation, *Desalination*, 263 (2010) 36–44.
- [3] A.M. Fadaei, M.H. Dehghani, S. Nasser, A.H. Mahvi, N. Rastkari, M. Shayeghi, Organophosphorous pesticides in surface water of Iran, *Bull. Environ. Contam. Toxicol.*, 88 (2012) 867–869.
- [4] M. Hiran, K.H. Sanaullah, The effect of endosulfanon the testes of bluegill fish, *Lepomis macrochirus*: a histopathological study, *Arch. Environ. Contam. Toxicol.*, 51 (2006) 149–51.
- [5] A. Karataş, Toxic effects of diazinon on adult individuals of *Drosophila melanogaster*, *J. Appl. Biol. Sci.*, 3 (2009) 102–108.
- [6] P. Moudgil, A. Sharma, A.K. Tiwari, Potentiation of spermicidal activity of 2,4-dichlorobenzamil by Lidocaine, *Indian J. Exp. Biol.*, 40 (2002) 1373–1377.
- [7] L. Saabia, E. Bustosobregon, Melanin prevent damage elicited by the organophosphorous pesticide diazinon on the mouse testis, *Ecotoxicol. Environ. Saf.*, 72 (2009) 938–942.
- [8] M.I. Yousef, K.S. Salehen, Protective role of isoflavones against the toxic effect of cypermethrin on semen quality and testosterone Levels of rabbits, *J. Environ. Sci. Health*, 38 (2003) 463–478.
- [9] Y. Tang, S. Luo, Y. Teng, C. Liu, X. Xu, X. Zhang, L. Chen, Efficient removal of herbicide 2,4-dichlorophenoxyacetic acid from water using Ag/reduced graphene oxide co-decorated TiO<sub>2</sub> nanotube arrays, *J. Hazard. Mater.*, 241 (2012) 323–330.
- [10] K. Del Ángel-Sanchez, O. Vázquez-Cuchillo, A. Aguilar-Elguezabal, A. Cruz-López, A. Herrera-Gómez, Photocatalytic degradation of 2,4-dichlorophenoxyacetic acid under visible

- light: effect of synthesis route, *Mater. Chem. Phys.*, 139 (2013) 423–430.
- [11] F. Ghanbari, M. Moradi, *Electrooxidation Processes for Dye Degradation and Colored Wastewater Treatment*, R.K. Gautam, M.C. Chattopadhyaya, Eds., *Advanced Nanomaterials for Wastewater Remediation*, CRC Press LLC, London, 2016, pp. 111–158.
- [12] N. Jaafarzadeh, F. Ghanbari, M. Ahmadi, M. Omidinasab, Efficient integrated processes for pulp and paper wastewater treatment and phytotoxicity reduction: permanganate, electro-Fenton and  $\text{Co}_3\text{O}_4$ /UV/peroxymonosulfate, *Chem. Eng. J.*, 308 (2017) 142–150.
- [13] N. Jaafarzadeh, M. Omidinasab, F. Ghanbari, Combined electrocoagulation and UV-based sulfate radical oxidation processes for treatment of pulp and paper wastewater, *Process Saf. Environ. Prot.*, 102 (2016) 462–472.
- [14] W.D. Oh, Z. Dong, T.T. Lim, Generation of sulfate radical through heterogeneous catalysis for organic contaminants removal: current development, challenges and prospects, *Appl. Catal. B*, 194 (2016) 169–201.
- [15] Y.H. Guan, J. Ma, X.C. Li, J.Y. Fang, L.W. Chen, Influence of pH on the formation of sulfate and hydroxyl radicals in the UV/peroxymonosulfate system, *Environ. Sci. Technol.*, 45 (2011) 9308–9314.
- [16] N. Jaafarzadeh, F. Ghanbari, M. Moradi, Photo-electro-oxidation assisted peroxymonosulfate for decolorization of acid brown 14 from aqueous solution, *Korean J. Chem. Eng.*, 32 (2015) 458–464.
- [17] H.T. Chandran, S. Thangavel, C.V. Jipsa, G. Venugopal, Study on inorganic oxidants assisted sonocatalytic degradation of Resazurin dye in presence of  $\beta\text{-SnWO}_4$  nanoparticles, *Mater. Sci. Semicond. Process.*, 27 (2014) 212–219.
- [18] X. Cheng, H. Liang, A. Ding, X. Tang, B. Liu, X. Zhu, Z. Gan, D. Wu, G. Li, Ferrous iron/peroxymonosulfate oxidation as a pretreatment for ceramic ultrafiltration membrane: control of natural organic matter fouling and degradation of atrazine, *Water Res.*, 113 (2017) 32–41.
- [19] F. Ghanbari, M. Moradi, M. Manshour, Textile wastewater decolorization by zero valent iron activated peroxymonosulfate: compared with zero valent copper, *J. Environ. Chem. Eng.*, 2 (2014) 1846–1851.
- [20] B.T. Zhang, Y. Zhang, Y.G. Teng, M. Fan, Sulfate radical and its application in decontamination technologies, *Crit. Rev. Environ. Sci. Technol.*, 45 (2015) 1756–1800.
- [21] F.I. Hai, K. Yamamoto, K. Fukushi, Hybrid treatment systems for dye wastewater, *Crit. Rev. Environ. Sci. Technol.*, 37 (2007) 315–377.
- [22] J.J. Pignatello, E. Oliveros, A. MacKay, Advanced oxidation processes for organic contaminant destruction based on the Fenton reaction and related chemistry, *Crit. Rev. Environ. Sci. Technol.*, 36 (2006) 1–84.
- [23] M. Munoz, Z.M. Pedro, J.A. Casas, J.J. Rodriguez, Preparation of magnetite-based catalysts and their application in heterogeneous Fenton oxidation—a review, *Appl. Catal., B*, 176 (2015) 249–265.
- [24] F. Ghanbari, M. Moradi, Application of peroxymonosulfate and its activation methods for degradation of environmental organic pollutants: review, *Chem. Eng. J.*, 310 (2017) 41–62.
- [25] P. Hu, M. Long, Cobalt-catalyzed sulfate radical-based advanced oxidation: a review on heterogeneous catalysts and applications, *Appl. Catal., B*, 181 (2016) 103–117.
- [26] J. He, X. Yang, B. Men, D. Wang, Interfacial mechanisms of heterogeneous Fenton reactions catalyzed by iron-based materials: a review, *J. Environ. Sci.*, 39 (2016) 97–109.
- [27] D. Wan, W. Li, G. Wang, L. Lu, X. Wei, Degradation of p-nitrophenol using magnetic  $\text{Fe}^0/\text{Fe}_3\text{O}_4$ /coke composite as a heterogeneous Fenton-like catalyst, *Sci. Total Environ.*, 574 (2017) 1326–1334.
- [28] H.T. Dang, T.M.T. Nguyen, S.Q. Thi, T.T. Nguyen, Magnetic  $\text{CuFe}_2\text{O}_4$  prepared by polymeric precursor method as a reusable heterogeneous Fenton-like catalyst for the efficient removal of methylene blue, *Chem. Eng. Commun.*, 203 (2016) 1260–1268.
- [29] V.K. Garg, V.K. Sharma, E. Kuzmann, Purification of water by ferrites—mini review, ferrites and ferrates: chemistry and applications in sustainable energy and environmental remediation, *ACS Publ.*, 1 (2016) 137–143.
- [30] T. Zhang, H. Zhu, J.-P. Croué, Production of sulfate radical from peroxymonosulfate induced by a magnetically separable  $\text{CuFe}_2\text{O}_4$  spinel in water: efficiency, stability, and mechanism, *Environ. Sci. Technol.*, 47 (2013) 2784–2791.
- [31] L. Zou, Q. Wang, X. Shen, Z. Wang, M. Jing, Z. Luo, Fabrication and dye removal performance of magnetic  $\text{CuFe}_2\text{O}_4$ @ $\text{CeO}_2$  nanofibers, *Appl. Surf. Sci.*, 332 (2015) 674–681.
- [32] X. Zhang, M. Feng, R. Qu, H. Liu, L. Wang, Z. Wang, Catalytic degradation of diethyl phthalate in aqueous solution by persulfate activated with nano-scaled magnetic  $\text{CuFe}_2\text{O}_4$ /MWCNTs, *Chem. Eng. J.*, 301 (2016) 1–11.
- [33] F. Qi, W. Chu, B. Xu, Ozonation of phenacetin in associated with a magnetic catalyst  $\text{CuFe}_2\text{O}_4$ : the reaction and transformation, *Chem. Eng. J.*, 262 (2015) 552–562.
- [34] T. Zhang, Y. Chen, T. Leiknes, Oxidation of refractory benzothiazoles with PMS/ $\text{CuFe}_2\text{O}_4$ : kinetics and transformation intermediates, *Environ. Sci. Technol.*, 50 (2016) 1–11.
- [35] N.M. Mahmoodi, Photocatalytic ozonation of dyes using copper ferrite nanoparticle prepared by co-precipitation method, *Desalination*, 279 (2011) 332–337.
- [36] F.G. Nematollah Jaafarzadeh, M. Ahmadi, Efficient degradation of 2,4-dichlorophenoxyacetic acid by peroxymonosulfate/magnetic copper ferrite nanoparticles/ozone: a novel combination of advanced oxidation processes, *Chem. Eng. J.*, 320 (2017) 1–12.
- [37] APHA, *Standard Methods for the Examination of Water and Wastewater*, 20th ed., APHA, Washington, DC, 1999.
- [38] A.I. Vogel, *Vogel's Textbook of Quantitative Chemical Analysis*, Longman Scientific & Technical, London, 1989.
- [39] Y. Wang, H. Sun, H.M. Ang, M.O. Tade, S. Wang, Synthesis of magnetic core/shell carbon nanosphere supported manganese catalysts for oxidation of organics in water by peroxymonosulfate, *J. Colloid Interface Sci.*, 433 (2014) 68–75.
- [40] Y. Wang, H. Sun, H.M. Ang, M.O. Tade, S. Wang, Magnetic  $\text{Fe}_3\text{O}_4$ /carbon sphere/cobalt composites for catalytic oxidation of phenol solutions with sulfate radicals, *Chem. Eng. J.*, 245 (2014) 1–9.
- [41] P. Jing, J. Li, L. Pan, J. Wang, X. Sun, Q. Liu, Efficient photocatalytic degradation of acid fuchsin in aqueous solution using separate porous tetragonal- $\text{CuFe}_2\text{O}_4$  nanotubes, *J. Hazard. Mater.*, 284 (2015) 163–170.
- [42] Y.S. Jung, W.T. Lim, J.Y. Park, Y.H. Kim, Effect of pH on Fenton and Fenton-like oxidation, *Environ. Technol.*, 30 (2009) 183–190.
- [43] Q. Chen, F. Ji, T. Liu, P. Yan, W. Guan, X. Xu, Synergistic effect of bifunctional Co-TiO<sub>2</sub> catalyst on degradation of Rhodamine B: Fenton-photo hybrid process, *Chem. Eng. J.*, 229 (2013) 57–65.
- [44] N. Yang, J. Cui, L. Zhang, W. Xiao, A.N. Alshwabkeh, X. Mao, Iron electrolysis-assisted peroxymonosulfate chemical oxidation for the remediation of chlorophenol-contaminated groundwater, *J. Chem. Technol. Biotechnol.*, 91 (2016) 938–947.
- [45] Y.H. Huang, Y.F. Huang, C.I. Huang, C.Y. Chen, Efficient decolorization of azo dye Reactive Black B involving aromatic fragment degradation in buffered  $\text{Co}^{2+}$ /PMS oxidative processes with a ppb level dosage of  $\text{Co}^{2+}$ -catalyst, *J. Hazard. Mater.*, 170 (2009) 1110–1118.
- [46] J. Sun, M. Song, J. Feng, Y. Pi, Highly efficient degradation of ofloxacin by UV/Oxone/ $\text{Co}^{2+}$  oxidation process, *Environ. Sci. Pollut. Res.*, 19 (2012) 1536–1543.
- [47] J.H. Sun, S.P. Sun, J. Sun, R.X. Sun, L.P. Qiao, H.Q. Guo, M.H. Fan, Degradation of azo dye Acid black 1 using low concentration iron of Fenton process facilitated by ultrasonic irradiation, *Ultrason. Sonochem.*, 14 (2007) 761–766.
- [48] S. Akbari, F. Ghanbari, M. Moradi, Bisphenol A degradation in aqueous solutions by electrogenerated ferrous ion activated ozone, hydrogen peroxide and persulfate: applying low current density for oxidation mechanism, *Chem. Eng. J.*, 294 (2016) 298–307.

- [49] L. Guo, J. Ding, M. Ou, Q. Zhong, Low-temperature  $\text{NO}_x$  ( $x = 1, 2$ ) removal with  $\cdot\text{OH}$  radicals from catalytic ozonation over  $\alpha\text{-FeOOH}$ , *Ozone: Sci. Eng.*, 38 (2016) 382–394.
- [50] S.K. Ling, S. Wang, Y. Peng, Oxidative degradation of dyes in water using  $\text{Co}^{2+}/\text{H}_2\text{O}_2$  and  $\text{Co}^{2+}$ /peroxymonosulfate, *J. Hazard. Mater.*, 178 (2010) 385–389.
- [51] J. Madhavan, P. Maruthamuthu, S. Murugesan, M. Ashokkumar, Kinetics of degradation of acid red 88 in the presence of  $\text{Co}^{2+}$ -ion/peroxomonosulphate reagent, *Appl. Catal., A*, 368 (2009) 35–39.
- [52] J. Madhavan, B. Muthuraaman, S. Murugesan, S. Anandan, P. Maruthamuthu, Peroxomonosulphate, an efficient oxidant for the photocatalysed degradation of a textile dye, acid red 88, *Sol. Energy Mater. Solar Cells*, 90 (2006) 1875–1887.
- [53] Y. Yang, J. Jiang, X. Lu, J. Ma, Y. Liu, Production of sulfate radical and hydroxyl radical by reaction of ozone with peroxymonosulfate: a novel advanced oxidation process, *Environ. Sci. Technol.*, 49 (2015) 25–34.
- [54] N. Jaafarzadeh, F. Ghanbari, M. Ahmadi, Efficient degradation of 2,4-dichlorophenoxyacetic acid by peroxymonosulfate/magnetic copper ferrite nanoparticles/ozone: a novel combination of advanced oxidation processes, *Chem. Eng. J.*, 320 (2017) 436–447.
- [55] J.L. Rodríguez, M.A. Valenzuela, H. Tiznado, T. Poznyak, I. Chaírez, D. Magallanes, A comparative study of alumina-supported Ni catalysts prepared by photodeposition and impregnation methods on the catalytic ozonation of 2,4-dichlorophenoxyacetic acid, *J. Nano Res.*, 19 (2017) 41–54.
- [56] B. Ying, G. Lin, L. Jin, Y. Zhao, T. Zhang, J. Tang, Adsorption and degradation of 2,4-dichlorophenoxyacetic acid in spiked soil with  $\text{Fe}^0$  nanoparticles supported by biochar, *Acta Agric. Scand. Sect. B*, 65 (2015) 215–221.
- [57] Y. Yao, Y. Cai, F. Lu, F. Wei, X. Wang, S. Wang, Magnetic recoverable  $\text{MnFe}_2\text{O}_4$  and  $\text{MnFe}_2\text{O}_4$ -graphene hybrid as heterogeneous catalysts of peroxymonosulfate activation for efficient degradation of aqueous organic pollutants, *J. Hazard. Mater.*, 270 (2014) 61–70.
- [58] X. Liu, Z. Zhou, G. Jing, J. Fang, Catalytic ozonation of Acid Red B in aqueous solution over a Fe–Cu–O catalyst, *Sep. Purif. Technol.*, 115 (2013) 129–135.
- [59] Y. Nie, S. Xing, C. Hu, J. Qu, Efficient removal of toxic pollutants over Fe–Co/ZrO<sub>2</sub> bimetallic catalyst with ozone, *Catal. Lett.*, 142 (2012) 1026–1032.
- [60] P.R. Shukla, S. Wang, H. Sun, Activated carbon supported cobalt catalysts for advanced oxidation of organic contaminants in aqueous solution, *Appl. Catal., B*, 100 (2010) 529–534.
- [61] P. Shi, R. Su, S. Zhu, M. Zhu, D. Li, S. Xu, Supported cobalt oxide on graphene oxide: highly efficient catalysts for the removal of Orange II from water, *J. Hazard. Mater.*, 229 (2012) 331–339.
- [62] Y. Yao, C. Xu, J. Qin, Synthesis of magnetic cobalt nanoparticles anchored on graphene nanosheets and catalytic decomposition of orange II, *Ind. Eng. Chem. Res.*, 52 (2013) 17341–17350.
- [63] F.J. Beltran, *Ozone Reaction Kinetics for Water and Wastewater Systems*, CRC Press, Boca Raton, FL, 2003.
- [64] F.J. Beltran, F.J. Rivas, R. Montero-de-Espinosa, Catalytic ozonation of oxalic acid in an aqueous TiO<sub>2</sub> slurry reactor, *Appl. Catal., B*, 39 (2002) 221–231.
- [65] Y.H. Guan, J. Ma, Y.M. Ren, Y.L. Liu, J.Y. Xiao, L. Lin, C. Zhang, Efficient degradation of atrazine by magnetic porous copper ferrite catalyzed peroxymonosulfate oxidation via the formation of hydroxyl and sulfate radicals, *Water Res.*, 47 (2013) 5431–5438.
- [66] F. Ji, C. Li, L. Deng, Performance of CuO/oxone system: heterogeneous catalytic oxidation of phenol at ambient conditions, *Chem. Eng. J.*, 178 (2011) 239–243.
- [67] Y. Feng, D. Wu, Y. Deng, T. Zhang, K. Shih, Sulfate radical-mediated degradation of sulfadiazine by  $\text{CuFeO}_2$  rhombohedral crystal-catalyzed peroxymonosulfate: synergistic effects and mechanisms, *Environ. Sci. Technol.*, 50 (2016) 3119–3127.
- [68] W.D. Oh, S.K. Lua, Z. Dong, T.T. Lim, Performance of magnetic activated carbon composite as peroxymonosulfate activator and regenerable adsorbent via sulfate radical-mediated oxidation processes, *J. Hazard. Mater.*, 284 (2015) 1–9.
- [69] J. Lu, X. Wei, Y. Chang, S. Tian, Y. Xiong, Role of Mg in mesoporous  $\text{MgFe}_2\text{O}_4$  for efficient catalytic ozonation of Acid Orange II, *J. Chem. Technol. Biotechnol.*, 91 (2015) 985–993.
- [70] J. Nawrocki, B. Kasprzyk-Hordern, The efficiency and mechanisms of catalytic ozonation, *Appl. Catal., B*, 99 (2010) 27–42.
- [71] J. Sharma, I.M. Mishra, D.D. Dionysiou, V. Kumar, Oxidative removal of Bisphenol A by UV-C/peroxymonosulfate (PMS): kinetics, influence of co-existing chemicals and degradation pathway, *Chem. Eng. J.*, 276 (2015) 193–204.
- [72] Y. Wang, W. Chu, Degradation of a xanthene dye by Fe(II)-mediated activation of oxone process, *J. Hazard. Mater.*, 186 (2011) 1455–1461.
- [73] M. Muthukumar, N. Selvakumar, Studies on the effect of inorganic salts on decolouration of acid dye effluents by ozonation, *Dyes Pigm.*, 62 (2004) 221–228.
- [74] J. Zhou, D. Xiao, Y. Guo, C. Fang, X. Lou, Z. Wang, J. Liu, Transformations of chloro and 1051 nitro groups during the peroxymonosulfate-based oxidation of 4-chloro-2-nitrophenol, *Chemosphere*, 134 (2015) 6–11.
- [75] Z. Wang, Y. Guo, L. Xu, J. Liu, Effects of chloride ions on bleaching of azo dyes by 1049  $\text{Co}^{2+}$ /oxone reagent: kinetic analysis, *J. Hazard. Mater.*, 190 (2011) 1083–1087.
- [76] S. Naumov, G. Mark, C. Sonntag, The reactions of nitrite ion with ozone in aqueous solution – new experimental data and quantum-chemical considerations, *Ozone: Sci. Eng.*, 32 (2010) 430–434.
- [77] Y. Ji, C. Dong, D. Kong, J. Lu, New insights into atrazine degradation by cobalt catalyzed peroxymonosulfate oxidation: kinetics, reaction products and transformation mechanisms, *J. Hazard. Mater.*, 285 (2015) 491–500.
- [78] P. Neta, R.E. Huie, A.B. Ross, Rate constants for reactions of inorganic radicals in aqueous solution, *J. Phys. Chem. Ref. Data*, 17 (1988) 1027–1284.
- [79] Y. Ji, Y. Fan, K. Liu, D. Kong, J. Lu, Thermo activated persulfate oxidation of antibiotic sulfamethoxazole and structurally related compounds, *Water Res.*, 87 (2015) 1–9.
- [80] F. Qi, W. Chu, B. Xu, Modeling the heterogeneous peroxymonosulfate/Co-MCM41 process for the degradation of caffeine and the study of influence of cobalt sources, *Chem. Eng. J.*, 235 (2014) 10–18.
- [81] G.P. Anipsitakis, D.D. Dionysiou, Radical generation by the interaction of transition metals with common oxidants, *Environ. Sci. Technol.*, 38 (2004) 3705–3712.
- [82] T. Zeng, X. Zhang, S. Wang, H. Niu, Y. Cai, Spatial confinement of a  $\text{Co}_3\text{O}_4$  catalyst in hollow metal–organic frameworks as a nanoreactor for improved degradation of organic pollutants, *Environ. Sci. Technol.*, 49 (2015) 2350–2357.
- [83] M. Ahmadi, F. Ghanbari, M. Moradi, Photocatalysis assisted by peroxymonosulfate and persulfate for benzotriazole degradation: effect of pH on sulfate and hydroxyl radicals, *Water Sci. Technol.*, 72 (2015) 2095–2102.
- [84] Y. Zhou, J. Jiang, Y. Gao, J. Ma, S.Y. Pang, J. Li, X.T. Lu, L.P. Yuan, Activation of peroxymonosulfate by benzoquinone: a novel nonradical oxidation process, *Environ. Sci. Technol.*, 49 (2015) 12941–12950.